Supplementary Material:

Multidisciplinary Design Modeling and Optimization for Satellite with Maneuver Capability

BY: Hai Huang, Haichao An, Wenrui Wu, Lingyan Zhang, Beibei Wu, Weipeng Li(✉)

Beihang University, Beijing 100191, China

liweipeng@buaa.edu.cn

1 velocity increments for Strategies 1 to 5

According to the Maneuver Strategies 1 to 5 listed in the article in Section 2.2.1, the velocity increment in each strategy is formulated as follows. For more details, refer to (Howard 2009).

Strategy 1 –The Hohmann transfer is a two-impulse maneuver for transferring between two coplanar orbits sharing a common focus, which is an elliptical orbit tangent to both circles at its apse line. The perigee and apogee of the transfer orbit are the radii of the initial and target orbits respectively, and only one-half of the ellipse is flown during the maneuver.

For circular and elliptical orbits, the velocities expressed as follow could be easily obtained.

$$v_{C1} = \sqrt{\mu / r_1}, \qquad v_{C2} = \sqrt{\mu / r_2}\,, \tag{1}$$

$$v_{e.p} = \sqrt{\frac{2\mu r_2}{r_1(r_1 + r_2)}}, \qquad v_{e.a} = \sqrt{\frac{2\mu r_1}{r_2(r_1 + r_2)}}\,, \tag{2}$$

where r_1 and r_2 are the radii of the parking orbit and target orbit respectively, v_{C1} and v_{C2} are the velocities of the parking orbit and target orbit respectively, $v_{e.p}$ and $v_{e.a}$ are the velocities of the ellipse at perigee and apogee respectively.

The velocity increment Δv_P during the 1st impulse to boost the satellite onto the higher-energy elliptical trajectory then could be expressed as

$$\Delta v_P = v_{e.p} - v_{C1} = \sqrt{\frac{\mu}{r_1}}\left(\sqrt{\frac{2r_2}{r_1+r_2}} - 1\right). \tag{3}$$

Then the velocity increment Δv_A for the 2nd impulse during the Hohmann transfer to place the satellite on the target orbit is

$$\Delta v_A = v_{C2} - v_{e.a} = \sqrt{\frac{\mu}{r_2}}\left(1 - \sqrt{\frac{2r_1}{r_1+r_2}}\right). \tag{4}$$

The total velocity increment for the Hohmann transfer then could be got as

$$\Delta v_1 = \Delta v_P + \Delta v_A = \sqrt{\frac{\mu}{r_1}}\left[\sqrt{\frac{2\gamma}{1+\gamma}} - 1 + \frac{1}{\sqrt{\gamma}}\left(1 - \sqrt{\frac{2}{1+\gamma}}\right)\right], \tag{5}$$

where $\gamma = r_2/r_1$.

Fig. 1 illustrates an orbit plane change through an angle ϑ between two circular orbits with the same radius. The velocity increment Δv is applied so as to rotate the velocity v_1 through this angle. The resulting velocity triangle is isosceles and from this triangle, the expression could be written as

$$\Delta v = 2v_1 \sin(\vartheta/2) = 2\sqrt{\mu/r}\sin(\vartheta/2), \tag{6}$$

where r is the radius of the two circular orbits. If the plane change maneuver is performed at an equatorial crossing, then the plane change angle ϑ is equal to the inclination change angle Δi.

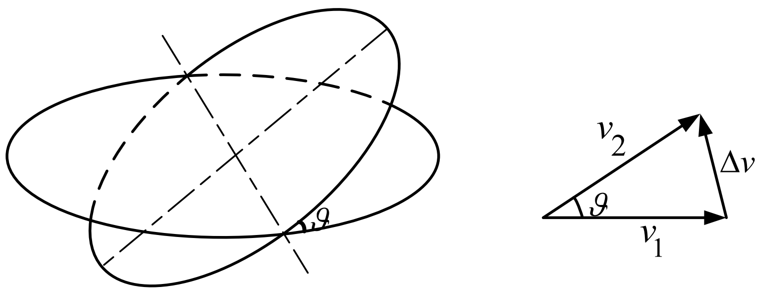

Fig. 1 Single impulse plane change for circular orbits and corresponding velocity vector triangle

So the velocity increment Δv_2 for the 3rd impulse in Strategy 1 is

$$\Delta v_2 = 2\sqrt{\mu/r_2}\,\sin(\vartheta/2). \tag{7}$$

Finally, the total velocity increment $\Delta v_{a,1}$ in Strategy 1 could be calculated as

$$\Delta v_{a,1}=\Delta v_1+\Delta v_2=\sqrt{\frac{\mu}{r_1}}\left[\sqrt{\frac{2\gamma}{1+\gamma}}-1+\frac{1}{\sqrt{\gamma}}(1-\sqrt{\frac{2}{1+\gamma}})\right]+2\sqrt{\frac{\mu}{r_2}}\sin(\frac{\vartheta}{2}). \tag{8}$$

Strategy 2 –The first step with a velocity impulse in Strategy 2 is the transfer from the perigee to the apogee and the velocity increment required for this impulse Δv_1 could be expressed like (3), then

$$\Delta v_1=\sqrt{\frac{\mu}{r_1}}(\sqrt{\frac{2r_2}{r_1+r_2}}-1). \tag{9}$$

Fig. 2 shows two orbits having a common focus F but not lying in a common plane and a plane change maneuver at apogee. And the plane change maneuver at perigee has the same feature with this. It could be obviously seen that the single impulse plane change illustrated in Fig. 1 is a special case for plane changes shown in Fig. 2. According to the velocity vector triangle and the law of cosines, we see that the magnitude of Δv needed for the plane change maneuver is

$$\Delta v=\sqrt{v_1^2+v_2^2-2v_1v_2\cdot\cos\delta}. \tag{10}$$

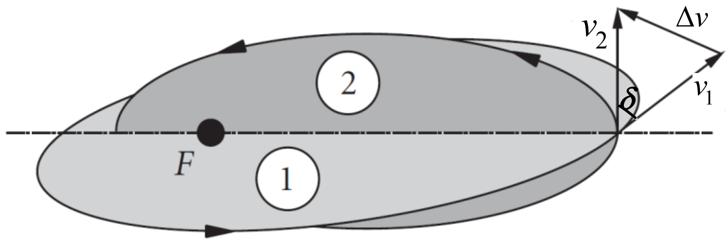

Fig. 2 Plane change at apogee

As both orbital transfers are conducted either at ascending node or descending node (i.e.in the equatorial plane), then the plane change angle equals to the corresponding inclination change angle. So the velocity increment for the 2nd impulse in Strategy 2 can be got as

$$\Delta v_2=\sqrt{\frac{\mu}{r_2}}\cdot\sqrt{\frac{3r_1+r_2}{r_1+r_2}-2\sqrt{\frac{2r_1}{r_1+r_2}}\cdot\cos\Delta i}. \tag{11}$$

The total velocity increment $\Delta v_{a,2}$ in Strategy 2 then is expressed as

$$\Delta v_{a,2}=\Delta v_1+\Delta v_2=\sqrt{\frac{\mu}{r_1}}(\sqrt{\frac{2r_2}{r_1+r_2}}-1)+\sqrt{\frac{\mu}{r_2}}\cdot\sqrt{\frac{3r_1+r_2}{r_1+r_2}-2\sqrt{\frac{2r_1}{r_1+r_2}}\cdot\cos\Delta i}\ . \tag{12}$$

Strategy 3 – The 1st impulse in this strategy is similar as the 2nd impulse in Strategy 2, as illustrated in Fig. 2. Then the velocity increment is formulate as

$$\Delta v_1=\sqrt{\frac{\mu}{r_1}}\cdot\sqrt{\frac{3r_2+r_1}{r_1+r_2}-2\sqrt{\frac{2r_2}{r_1+r_2}}\cdot\cos\Delta i}\ . \tag{13}$$

The 2nd transfer is just the 2nd orbit maneuver in Hohmann transfer, so according to Eq.(4), the velocity increment here is

$$\Delta v_2=\sqrt{\frac{\mu}{r_2}}(1-\sqrt{\frac{2r_1}{r_1+r_2}})\ . \tag{14}$$

The total velocity increment needed is

$$\Delta v_{a,3}=\Delta v_1+\Delta v_2=\sqrt{\frac{\mu}{r_1}}\cdot\sqrt{\frac{3r_2+r_1}{r_1+r_2}-2\sqrt{\frac{2r_2}{r_1+r_2}}\cdot\cos\Delta i}+\sqrt{\frac{\mu}{r_2}}(1-\sqrt{\frac{2r_1}{r_1+r_2}})\ . \tag{15}$$

Strategy 4 –The inclination change angles in the 1st and 2nd impulse are δ and $\Delta i-\delta$, respectively. So the velocity increments Δv_1 and Δv_2 are

$$\Delta v_1=\sqrt{\frac{\mu}{r_1}}\cdot\sqrt{\frac{3r_2+r_1}{r_1+r_2}-2\sqrt{\frac{2r_2}{r_1+r_2}}\cdot\cos\delta}\ , \tag{16}$$

$$\Delta v_2=\sqrt{\frac{\mu}{r_2}}\cdot\sqrt{\frac{3r_1+r_2}{r_1+r_2}-2\sqrt{\frac{2r_1}{r_1+r_2}}\cdot\cos(\Delta i-\delta)}\ . \tag{17}$$

The total velocity increment in Strategy 4 is

$$\Delta v_{a,5}=\Delta v_1+\Delta v_2=\sqrt{\frac{\mu}{r_1}}\cdot\sqrt{\frac{3r_2+r_1}{r_1+r_2}-2\sqrt{\frac{2r_2}{r_1+r_2}}\cdot\cos\delta}+\sqrt{\frac{\mu}{r_2}}\cdot\sqrt{\frac{3r_1+r_2}{r_1+r_2}-2\sqrt{\frac{2r_1}{r_1+r_2}}\cdot\cos(\Delta i-\delta)} \tag{18}$$

Strategy 5 –The two orbital transfers are both orbit plane change, and the inclination change angles are both $\Delta i/2$. According to Eq.(10), the velocity increments Δv_1 and Δv_2 are written as follow

$$\Delta v_1=\sqrt{\frac{\mu}{r_1}}\cdot\sqrt{\frac{3r_2+r_1}{r_1+r_2}-2\sqrt{\frac{2r_2}{r_1+r_2}}\cdot\cos\frac{\Delta i}{2}}\ , \tag{19}$$

$$\Delta v_2=\sqrt{\frac{\mu}{r_2}}\cdot\sqrt{\frac{3r_1+r_2}{r_1+r_2}-2\sqrt{\frac{2r_1}{r_1+r_2}}\cdot\cos\frac{\Delta i}{2}}\ . \tag{20}$$

And the total velocity increment is calculated as

$$\Delta v_{a,4}=\Delta v_1+\Delta v_2=\sqrt{\frac{\mu}{r_1}}\cdot\sqrt{\frac{3r_2+r_1}{r_1+r_2}-2\sqrt{\frac{2r_2}{r_1+r_2}}\cdot\cos\frac{\Delta i}{2}}+\sqrt{\frac{\mu}{r_2}}\cdot\sqrt{\frac{3r_1+r_2}{r_1+r_2}-2\sqrt{\frac{2r_1}{r_1+r_2}}\cdot\cos\frac{\Delta i}{2}}\ . \tag{21}$$

2 Calculation of disturbance moments for control disciplinary

The calculation of disturbance moments in this section is based on accurate models, which are used to establish the corresponding approximate model for outside disturbance moments.

(1) Moment of gravity gradient

Under small angle perturbations, the momentum components of gravity gradient of a satellite in body-fixed coordinate system can be presented as

$$\begin{aligned} M_{gx} &= 3\omega_0^2(I_{zz}-I_{yy})\varphi \\ M_{gy} &= 3\omega_0^2(I_{zz}-I_{xx})\theta \ , \\ M_{gz} &= 0 \end{aligned} \tag{22}$$

where ω_0 is the angular velocity of orbit, I_{xx} , I_{yy} , I_{zz} are mass moments of inertias in *X*, *Y* and *Z* axes of body-fixed coordinate system respectively, φ and θ are roll angle and pitch angle respectively.

(2) Moment of aerodynamic force

Assuming the atmosphere rotation velocity is 1.5 times of that of the Earth, the momentum of aerodynamic force can be presented as

$$\begin{aligned} M_{ax} &= \frac{-\rho V_R^2}{2}C_D A_P l_z \alpha \\ M_{ay} &= \frac{-\rho V_R^2}{2}C_D A_P l_z \\ M_{az} &= \frac{\rho V_R^2}{2}C_D A_P (l_x\alpha + l_y) \ , \\ \alpha &= \frac{1.5\omega_e}{\omega_0}\sin i\cos\omega_0 t \end{aligned} \tag{23}$$

where ρ is orbital air density, V_R is relative velocity between satellite and air that can be approximately presented as $V_R = \sqrt{\frac{\mu}{h}(1-\frac{3\omega_e}{\omega_0}\cos i)}$; C_D is coefficient of drag, A_P is the face area; l_x, l_y, l_z are the components of radius vector l from mass center to aerodynamic force center in *X*, *Y* and *Z* axes of body-fixed coordinate system respectively, ω_e and ω_0 are the rotation velocities of the Earth and the orbit, i is the orbital inclination, and t is the time starting from ascending node.

(3) Moment of solar pressure

The momentum of solar pressure can be presented as below under perfect reflection assumption,

$$\boldsymbol{M}_{sa} = \boldsymbol{l}_p \times (2\frac{F_e}{c} \cdot A \cdot \boldsymbol{n}), \tag{24}$$

where A is the area of sunlit surface, F_e is the solar flux constant 1358W/m^2; c is the light speed, $\boldsymbol{l}_p$ is radius vector form mass center to solar pressure center, and $\boldsymbol{n}$ is the unit normal vector of sunlit surface.

(4) Earth magnetic moment

The components of the Earth magnetic moment in *X*, *Y* and *Z* directions of body-fixed coordinate system can be stated as

$$\begin{aligned} T_{mx} &= M_{yb}B_{zb} - M_{zb}B_{yb} \\ T_{my} &= M_{zb}B_{xb} - M_{xb}B_{zb}, \\ T_{mz} &= M_{xb}B_{yb} - M_{yb}B_{xb} \end{aligned} \tag{25}$$

where B_{xb}, B_{yb} and B_{zb} as well as M_{xb}, M_{yb} and M_{zb} are respectively the components of Earth magnetic vector $\boldsymbol{B}$ and the satellite internal magnetic torque $\boldsymbol{M}$ in *X*, *Y* and *Z* directions of body-fixed coordinate system.

3 Supplementary analysis modeling for power disciplinary

3.1 Required power of satellite

The satellite consumed power can be regarded as permanent power P_0 and short-term power. The permanent power is constantly consumed. However, the short-term power is only consumed when the temporary working device(s) or payload(s) work, and it is usually divided into three types as below.

Type I it is only consumed in Earth shadow periods, and the power amount and duration time are P_{ma} and T_{ma} $(ma = 1, 2, 3, \cdots, N_{ma})$, where N_{ma} is the number of consumed times by temporary working device(s) in an Earth shadow period.

Type II it is only consumed in light periods, together with which the permanent power does not excess the total power provided by solar array. The power amount and duration time are P_{mc} and T_{mc} $(mc = 1, 2, 3, \cdots, N_{mc})$, where N_{mc} is the number of consumed times by temporary working device(s) in a light period.

Type III it is only consumed in light periods, together with which the permanent power excesses the total power provided by solar array. The power amount and duration time are P_{me} and T_{me} $(me = 1, 2, 3, \cdots, N_{me})$, where N_{me} is the number of consumed times by temporary working device(s) in a light period.

In this study, the power budget of the satellite subsystems and payload operations are given as Table 1.

Table 1 Power budget of satellite subsystems and payload operations

Subsystems/Operations		Permanent power	Short-term power	Power types
Platform	Thermal control	40	30	Type I
	Attitude control	100	0	
	Power	16	0	
	TT&C	22	0	
	DBDH	30	0	
	Data transmission	15	60	Type I &II
Operations	Rendezvous measurement	67	0	
	Signal test	5	691	Type III
Total		295	781	

TT&C -- Tracking telemetry and command;

DBDH – On board data handle

There are three working modes A, B and C of the short-term power, i.e. mode A (**Type I**) – only thermal control device works during the whole Earth shadow period; mode B (**Types II and III**) – both data transmission and signal test devices work in light period, and the operating durations are 6 minutes and 9 minutes respectively; and mode C (**Type I**) – both thermal control and data transmission devices work in Earth shadow period, and the operating durations are T_e and 6 minutes respectively.

3.2 Fundamental relations for analysis of power disciplinary

(1) Angle between the sunlight ray and solar array

For sun-synchronous orbits, the orbital sun-angle η can be presented as (Wang 1995)

$$\cos\eta = \cos i \sin\delta_h - \sin i \cos\delta_h \sin(\alpha_h - \Omega_0 - Day/365\cdot 2\pi) \quad Day \in [0,365], \quad (26)$$

where *Day* is the number of days counted from the vernal equinox moment, and Ω_0 is the ascending node at the vernal equinox moment. The right ascension α_h and declination δ_h of the sun can be presented as

$$\begin{aligned} \tan\alpha_h &= \cos\varepsilon \tan\Lambda \\ \sin\delta_h &= \sin\varepsilon \sin\Lambda \end{aligned}, \quad (27)$$

where ε is the obliquity of the ecliptic which is $23^{\circ}26'$, and celestial longitude is taken as $\Lambda = Day/365\cdot 2\pi$.

Because the attitude angles of the designed satellite is quite small, the normal direction of solar panels can be taken as perpendicular to the normal direction of orbit plane, meanwhile it is adjusted through rotating axis to always point along the projection of radius vector to the sun in the orbital plane. Therefore the angle between the sunlight ray and the normal direction of solar panels is just the orbital sun-angle η.

(2) Earth shadow period

For circular orbits, the ratio of the Earth shadow period T_e to orbital period *T*, or k_e can be presented as the following formula (Xiao 1995), which is used to determine the period T_e.

$$k_e = \frac{T_e}{T} = \begin{cases} \dfrac{1}{\pi}\arccos(\dfrac{\cos\alpha_0}{\sin\eta}) & \cos\alpha_0 \le \sin\eta \\ 0 & \cos\alpha_0 > \sin\eta \end{cases}, \quad (28)$$

where

$$\cos\alpha_0 = \frac{\sqrt{2R_e h + h^2}}{R_e + h}. \quad (28)$$

(3) Energy balance of battery group

During the shadow period in an orbit circle, the solar array does not work, and the discharged energy of battery group can be presented as

$$Q_{Fe} = \frac{P_0 \cdot T_e + \sum_{ma}^{N_{ma}} P_{ma} \cdot T_{ma}}{F_1 \cdot \eta_D}, \tag{30}$$

where F_1 is the loss factor of discharging circuit; η_D is the efficiency of the discharging adjustor.

During the light period in an orbit circle, the solar array works and provides output power which includes the permanent power P_0 as well as the remained part P_c to charge battery group or consumed by short-term devices, therefore the discharged energy of battery group in the period can be calculated as

$$Q_{Fd} = \frac{\sum_{me}^{N_{me}} P_{me} \cdot T_{me}}{F_1 \cdot \eta_D} - P_c \cdot \sum_{me}^{N_{me}} T_{me}. \tag{31}$$

On the other hand during the phase when no short-term power is consumed in a light period, the charged energy of battery group can be calculated as

$$Q_{C0} = P_c \cdot (T_d - \sum_{mc}^{N_{mc}} T_{mc} - \sum_{me}^{N_{me}} T_{me}) \cdot F_t \cdot \eta_{wh} \cdot \eta_c, \tag{32}$$

where T_d is the light period, $T_d = T - T_e$; F_t is the chargeable time proportion in the light period; η_{wh} is the charging efficiency; and η_c is the efficiency of the discharging adjustor.

Meanwhile during the phase when short-term power **Type II** is consumed in a light period, the additional charged energy of battery group can be calculated as

$$Q_{C1} = (P_c \sum_{mc=1}^{N_{mc}} T_{mc} - \frac{\sum_{mc=1}^{N_{mc}} P_{mc} \cdot T_{mc}}{F_1 \cdot \eta_D}) \cdot \eta_{wh} \cdot \eta_c. \tag{33}$$

Summating the charged and discharged energies, the electrical energy margin of the battery group in an orbit circle can be obtained as

$$Q_{DF} = Q_{C0} + Q_{C1} - Q_{Fe} - Q_{Fd}. \tag{34}$$

Q_{DF} changes vs. different orbit circles due to working mode change, hereby using $Q_{DFi} (i = 1, \cdots, n)$ to present Q_{DF} in the *i*-th orbit, therefore it comes to the equation of battery energy balance in *n* orbit circles (*n*=14 in this study)

$$\sum_{i=1}^{n} Q_{DFi} = 0 . \tag{35}$$

(4) Solar array power in end of lifetime

In early days, the output power of solar array P_{BOL} can be presented as (Ma 2001)

$$P_{BOL} = S_0 X X_s X_e A_s \bar{\eta} F_c (\beta_P \Delta T + 1) \cos\eta , \tag{35}$$

where S_0 is the solar constant, taken the value 1353 W/cm^2; η is the angle between the sunlight ray and the normal direction of solar array; X is the correction factor for shine sideways, in a range of 0.95~1.00; X_s is a factor for season change, taken 1.0 at vernal or autumnal equinox, 0.9637 at summer solstice and 1.3027 at winter solstice; X_e is a gain factor considering the light reflection from the Earth, taken 1 for geosynchronous orbit and 1~1.05 for others; A_s is the total area of solar cell; $\bar{\eta}$ is photoelectric conversion efficiency of the solar cell; F_c is the cell assembling loss factor; β_P is the power thermal coefficient; and ΔT is the temperature difference between orbit and standard environments; and

$$A_s = A_{sa} F_j , \tag{36}$$

where F_j is the coefficient of cell distribution. For the parameters which are not given specified values in the study, they are all between 0.9~1.0, which should be set according to the need of practical application.

4 Analysis modeling for structural disciplinary

Based on the initial design of the satellite structure with folded solar panels, an FE model was established, which is mainly composed of shell, beam and rod elements. In the model construction, the honeycomb panels are simplified as composite shells with equivalent thicknesses, which are directly connected with other structural panels by equivalent nodes. The mass of the onboard devices is modeled in the FE model by nonstructural mass (NSM) linked to the structure according to corresponding layouts. Eighty percent of the propellant mass is set as two point mass elements in each fuel tank (eight point mass elements in total), and the two elements are connected with other elements at their installation position using the rigid element RBE2. The rest twenty percent of mass is constructed with NSM linked to the tank shells. As for the structural materials and material properties, they are listed in Tables 2 and 3. Based on the connecting interface between the satellite and launch vehicle, the boundary condition is to fix the bottom of the joint ring. MSC.Nastran is utilized to conduct the structural analysis, and the 1st order natural frequency for the whole satellite is about 22Hz.

Table 2 Material properties

Types	Designations	Properties
Isotropic Materials	LD10	E=7.06E10Pa, ν=0.33, ρ=2800kg/m^3
	LY12	E=7.061E10Pa, ν=0.3, ρ=2780kg/m^3
	TC4	E=1.018E11Pa, ν=0.41, ρ=4420kg/m^3
Composite Materials	M55j	E_{11}=2.86E11Pa, E_{22}=7.4E9Pa, ν=0.3, G_{12}=4.6E9Pa, G_{23}=3.68E9Pa, G_{13}=3.68E9Pa, ρ=1600kg/m^3
	LF2-YH5X0.03	E_{11}=8.04E4Pa, E_{22}=8.04E4Pa, ν=0.33, G_{12}=1.508E4Pa, G_{23}=8.85E7Pa, G_{13}=5.9E7Pa, ρ=27kg/m^3
Composite Laminates	Honeycomb panel with Aluminum skins	(Symmetric) L_0=LF2-YH5X0.03, t_0=19mm, L_1=LY12, t_1=0.5mm
	Honeycomb panel with Carbon fiber skins	(Symmetric) L_0=LF2-YH5X0.03, t_0=19.4mm, θ_0=0°, L_1=M55j, t_1=0.08mm, θ_1=90°, L_2=M55j, t_2=0.08mm, θ_2=45°, L_3=M55j, t_3=0.08mm, θ_3=0°, L_4=M55j, t_4=0.08mm, θ_4=-45°.

Table 3 Structural materials

Structural Components		Material types
Payload cabin panels	Top panels	Honeycomb panel with Aluminum skins
	Side panels	
	Base panels	Honeycomb panel with Carbon fiber skins
	Clapboards	
Transition Module Panels		Honeycomb panel with Aluminum skins
Platform Panels	Base panels	Honeycomb panel with Aluminum skins
	Top Panels	Honeycomb panel with Carbon fiber skins
	Middle panels	
Beam Frame		M55j
Tanks		TC4
Joint Ring Shells		M55j
Joint Ring Frame		LD10

References

Howard DC (2009) Orbital mechanics for engineering students. Elsevier, The Netherlands

Ma S (2001) Satellite power technology. China Astronautical Publishing House, Beijing

Wang Y (1995) Calculation method of the incident angle of the Sun relative to the orbital plane in sun-synchronous orbit. Spacecraft Engineering 4 (4):65-73

Xiao Y (1995) Spacecraft dynamic theory. China Astronautical Publishing House, Beijing